Journal of Alloys and Compounds 509 (2011) 2631–2638

Contents lists available at ScienceDirect

Journal of Alloys and Compounds

journal homepage: www.elsevier.com/locate/jallcom

An approach to surface functionalization of indium tin oxide for regular growth of silver nano-particles and their optical features

Khalid Nouneh[a,b,*], Munetaka Oyama[b], Raquel Diaz[c], Mohammed Abd-Lefdil[d], I.V. Kityk[e], Mosto Bousmina[a]

[a] INANOTECH, Institute of Nanomaterials and Nanotechnology, MAScIR (Moroccan Advanced Science, Innovation and Research Foundation), ENSET, Av. Armée Royale, 10100, Rabat, Morocco
[b] Department of Material Chemistry, Graduate School of Engineering, Kyoto University, Nishikyo-ku, Kyoto 615-8520, Japan
[c] Departamento de Física Aplicada C-XII, Universidad Autónoma de Madrid, Madrid, Spain
[d] Department of Materials Physics, University Mohammed V, Rabat, Morocco
[e] Electrical Engineering Department, Czestochowa University of Technology, Armii Krajowej 17, Czestochowa, Poland

ARTICLE INFO

Article history:
Received 25 October 2010
Received in revised form
16 November 2010
Accepted 22 November 2010
Available online 1 December 2010

Keywords:
Silver nanoparticles
Surface functionalization
Indium tin oxide
Nano-structured material
UV–visible spectroscopy

ABSTRACT

A new strategy derived from seed-mediated growth was applied to attach and grow dense and uniform silver nanoparticles (AgNPs) on indium tin oxide (ITO) thin films deposited on glass substrate. This approach allowed obtaining narrower nanoparticle's size distribution and a much denser attachment compared with the classical seed-mediated growth method. Adjusting growth time permitted preparing relatively small and uniform Ag nanoparticles of less than 40 nm in size. The size, density and the regularity of AgNPs were found to be slightly affected by the nature of ITO substrate, which thus affects the plasmon absorbance spectra. The observed differences are attributed to the cavities existing between large grains and sub-grains of ITO thin films.

1. Introduction

During the recent years, intensive efforts have been devoted to the design of functional metal nanoparticles (NPs) due to their exciting and unique properties arising mainly from the "quantum size effect" with a wide spectrum of potential applications in catalysis, optics, electronics, sensing, biomaterials and biological and medical applications [1,2]. Among the targeted elements, silver (Ag) nanoparticles (AgNPs) are of importance due to their unique optical and antibacterial properties, excellent conductivity and chemical stability [3]. For instance, the unique optical properties of AgNPs originating from the excitation of the localized surface plasmon resonance (LSPR) have been applied in biochemical, medical diagnostics, and biological imaging [4].

Various synthetic strategies of AgNPs solutions have been reported such as chemical reduction of Ag ions in aqueous solutions with or without stabilizing agents [5–8], thermal decomposition in organic solvents [9], chemical- and photo-reduction in reverse micelles [10], radiation mediated chemical reduction [11] and microwave assisted synthesis [12]. By contrast, the assembly and the dispersion of AgNPs on planar surfaces have been only marginally addressed and due to important experimental difficulties and presence of a real challenge in films and nanoparticles fabrication. This requires a clear understanding of thin films fabrication, surface properties of the substrate as well as the chemistry and physical processes involved in the synthesis. Ghoranneviss et al. [13] fabricated Cu-NP deposited on different substrates such as glass, Al_2O_3 and SiO_2 and showed that uniform and nano-sized Cu nanoparticles can be produced on a lower-roughness substrate. Ulmeanu et al. [14] have also described the self-assembly process of silica colloidal particles for substrate surfaces implying mica, glass, Ag and Au thin films. For a constant solid concentration of colloidal particles, the quality of the self-assembled mono-layers was highly improved in rugged surface due to the large contact angle.

Because NPs are often used for the fabrication of specific devices with solid substrates, it is important to understand how the substrate affects their size and size distribution, spatial distribution

* Corresponding author at: INANOTECH, Institute of Nanomaterials and Nanotechnology, MAScIR (Moroccan Advanced Science, Innovation and Research Foundation), ENSET, Av. Armee Royale, 10100, Rabat, Morocco.
Tel.: +212 5 37 57 61 80; fax: +212 5 37 57 08 80.
E-mail addresses: k.nouneh@inanotech.mascir.com (K. Nouneh), iwank74@gmail.com (I.V. Kityk).

0925-8388/$ – see front matter © 2010 Elsevier B.V. All rights reserved.
doi:10.1016/j.jallcom.2010.11.172

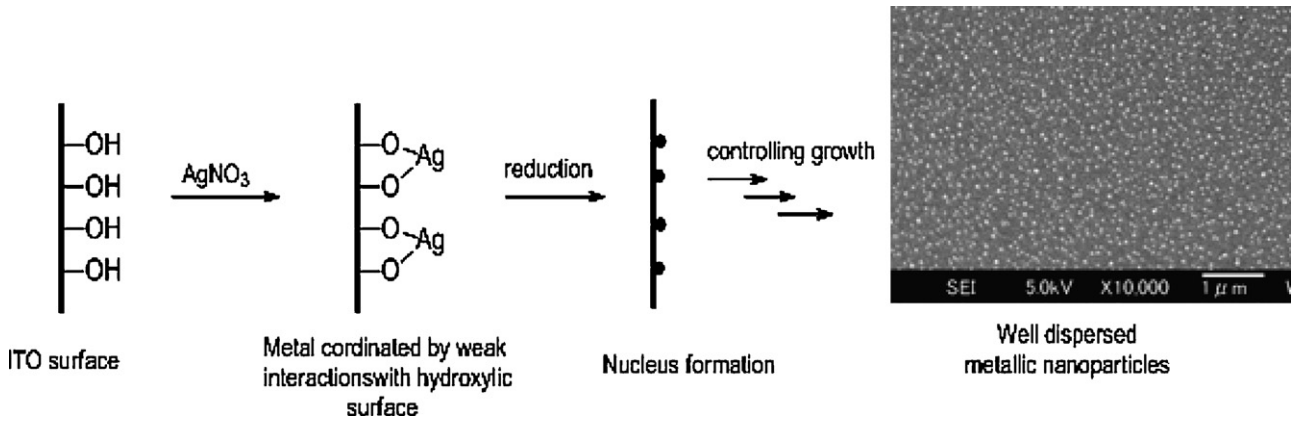

Scheme 1. A two step chemical modification procedure to create well attached and dispersed silver nanoparticles on indium tin oxide surface.

and optical properties. Of particular interest, indium tin oxide (ITO) matrices represent an attractive class of substrates due to their low electrical resistivity, high transparency in the visible range, and high reflectivity as well as low infrared emission in middle infrared region [15]. They are widely used as optically transparent electrodes in flat panel displays and in photovoltaic devices [16]. The more popular way to disperse AgNP on the ITO surface consists of the introduction of chelating ligands (aminopropyl, mercaptopropyl, etc.) by surface modification using the immersion of AgNP [17,18]. Unfortunately, this chemical functionalization causes an enhancement of electrochemical impedance, limiting thus their electrochemical transfer [6a,b].

Recently, we have investigated the electrochemistry of electron transfer dynamics of ferrocene terminated self-assembled monolayers (SAMs), co-adsorbed with single-walled carbon nanotube SWCNT on gold electrode [6c] and showed that the neighboring SWCNTs in the ferrocene molecular assemblies exert distinct impacts on the global electron transport and electrocatalytic behavior of the ferrocenes. The obtained results showed also that the presence of SWCNTs in the ferrocene assembly synergetically enhances the electrocatalytic detection of thiocyanate compared to pure ferrocene or pure SWCNTs. Looking for a more efficient alternative route; we recently examined the preparation of well controlled AgNPs with narrow size distribution by the normal seed-mediated growth method [6a]. However, the density and the size distribution of AgNPs were irregular and the resulting material suffered important inhomogeneity. To circumvent these limitations, we decided to revisit the seeding approach aiming at achieving a dense attachment of regular AgNPs size on ITO substrate. This is particularly important for the photoinduced nonlinear optical research [19,20].

In this work, a new strategy derived from seed-mediated growth method was developed allowing the fabrication of homogeneous dense and uniform AgNPs on ITO substrate with a sheet resistivity ca. 71 Ω/sq (ITO-A). Inspired by the reactivity of silica materials [21], we decided to simplify the strategy by introducing first the metallic silver nitrate, $AgNO_3$, on the surface followed by its reduction and growth. In addition, the effect of ITO substrate characteristics on the attached AgNPs size and regularity was examined. The behavior of these photoactive materials is discussed in terms of the AgNPs size regularity and density as well as ITO features based on their UV–visible absorbance spectra.

2. Experimental

We have chosen three types of ITO substrates. They were purchased from CBC Ings. Co. Ltd., Japan. ITO-A is produced by Asahi Beer Optical, Ltd., Japan, on a glass substrate with surface resistivity of about 71.5 Ω/sq while ITO-B and ITO-C, with low resistivity 3.6 and 1.9 Ω/sq, respectively, were obtained from Kuramoto Seisakusho Co. Ltd., Japan. The ITO films thickness was equal to 120 ± 12 nm, 215 ± 21 nm and 330 ± 25 nm for ITO-A, ITO-B and ITO-C, respectively.

A piece of ITO cut into a dimension of ca. 1 cm × 1 cm was used for each treatment. It was cleaned by sonication in acetone and in ethanol for 15 min each. After flushing by pure water, it was then cleaned by sonication in ultra pure water for an additional 15 min. This procedure was repeated twice to reach the desired effect. Finally, the ITO piece was dried with a stream of nitrogen gas before use.

AgNPs-attached on ITO substrates were prepared using the two-step chemical treatment.

In the first step, a piece of ITO was put in a solution that contains 0.5 ml of 0.01 M $AgNO_3$, 0.5 ml of 0.01 M trisodium citrate, $Na_3C_6H_5O_7$, and 20 ml of pure water. Then, 0.5 ml ice-cold of 0.1 M sodium borohydride, $NaBH_4$, aqueous solution was added into the solution to reduce Ag^+. In the second step, the Ag seed-particle modified ITO was immersed in a growth solution containing 0.5 ml of 0.01 M $AgNO_3$, 0.5 ml of 0.1 M cetyltrimethylammonium bromide, CTAB, 0.1 ml of 0.1 M ascorbic acid, $C_6H_8O_6$, and 0.1 ml of 1 M sodium hydroxide, NaOH, during various time intervals (0, 30 min, 1 h, 2 h, 3 h, 4 h, 6 h and 12 h) at a controlled temperature of 28 °C. During the growth time, the substrate color changed from colorless to deep-yellow upon reduction.

The solutions were prepared using pure water obtained from a water purification system Autopure WR600A, Yamato Co. Ltd., with a resistivity higher than 18 MΩ. $AgNO_3$ and CTAB were purchased from Aldrich Co. Ltd. $Na_3C_6H_5O_7$, $C_6H_8O_6$, $NaBH_4$ and NaOH solutions were obtained from Wako Pure Chemicals, Ltd.

The size and the morphology of the Ag nanoparticles attached to the ITO surface were characterized by field emission scanning electron microscopy (FE-SEM, JSM-7400F; JEOL, Japan) and SEIKO SPA-400 atomic force microscopy (AFM) in tapping mode. The optical spectrophotometer, U4100 Hitachi Ltd., Japan, was used to determine the absorption spectra of AgNPs/ITO within the spectral range 300–900 nm with the spectral resolution 1 nm, at room temperature. A comparative study of the amount of Sn dopant in the samples was analyzed with Energy Dispersive X-ray Analysis (EDAX). The contact angle measurements were performed using a JY-82 contact angle goniometer by the sessile drop technique at room temperature. The ITO sheet resistance was measured using the four point probe method for all substrates before (R_{S1}) and after (R_{S2}) AgNPs growth. The resistivity was computed from $\rho = R_S \times d$, where d is the film thickness. The grazing X-ray diffraction (GXRD) was performed in XïPert PRO, θ/θ, using an incidence angle of 1°.

3. Results and discussion

By applying the seed mediated growth method pioneered by Murphy and co-workers for preparing Au nanorods in solution [22], it was possible to attach AgNPs simply via the two-step immersion of ITO substrates in $AgNO_3$-based solutions; first, in a seed solution, and then, in a growth solution [6a]. However, the irregularity in terms of size and shape of the metallic nanoparticles and their low density constituted serious limitations. We anticipated that the introduction of the starting precursor ($AgNO_3$) before reduction may reduce the problems related to the heterogeneous structure of the material. Hence, we adopted a modified strategy based on the immersion of ITO substrate in a solution of $AgNO_3$ in the presence of a stabilizer (trisodium citrate) and ultra-pure water (see Section 2). As ITO surface features contains various hydroxyl groups, they will react upon immersion with Ag^+ allowing Ag cations to be chelated on the ITO surface. The weakly attached Ag cations were

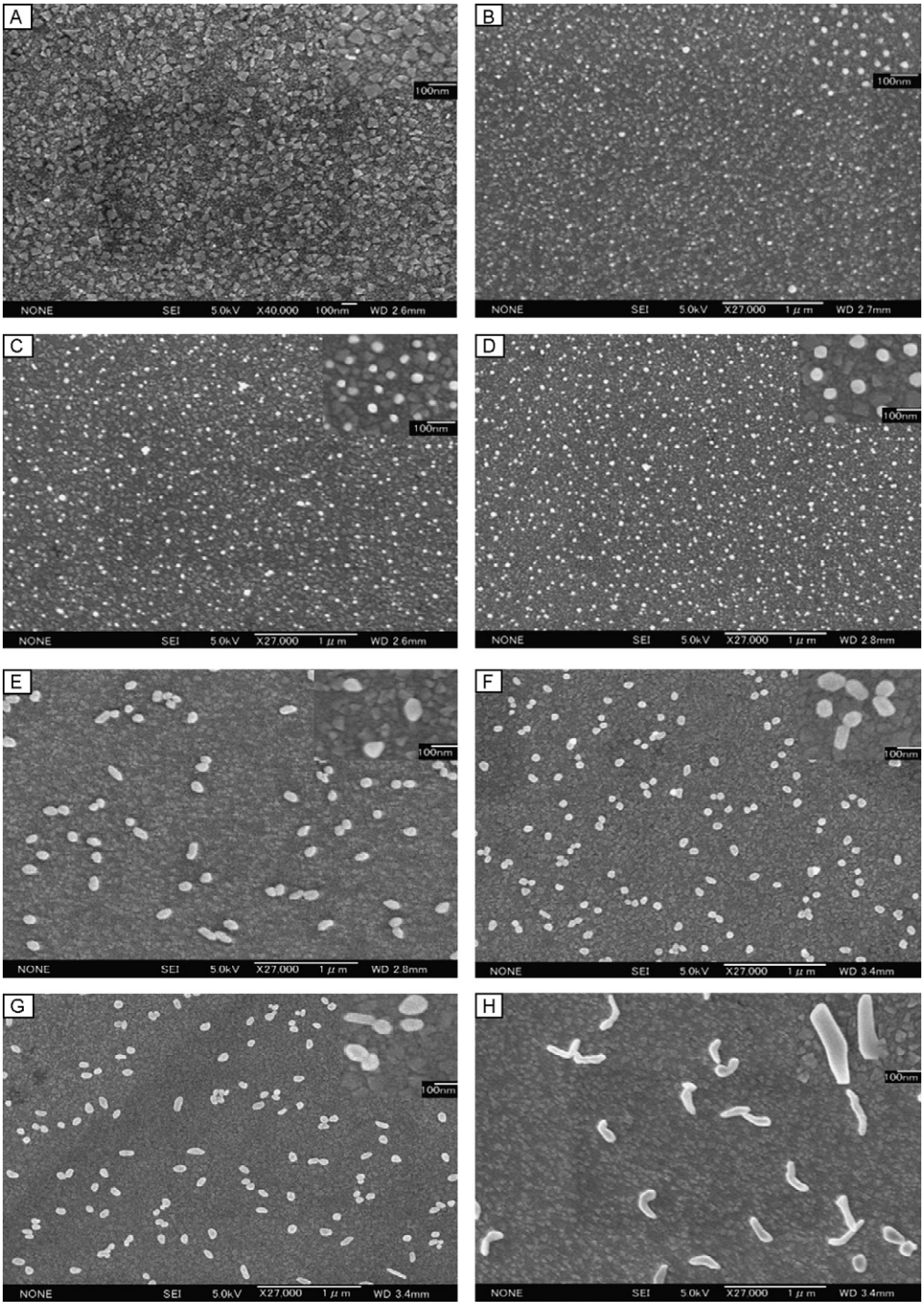

Fig. 1. SEM images of AgNPs/ITO-A surface prepared by the present seed-mediated growth method. The growth time was (A) 0, (B) 30 min, (C) 1 h, (D) 2 h, (E) 3 h, (F) 4 h, (G) 6 h and (H) 12 h, respectively, at 28 °C.

then reduced by $NaBH_4$, which results in a homogeneous dispersion of the Ag particles on the substrate surface. The summary of the AgNPs formation mechanism is illustrated in Scheme 1. The functionalized substrates were then immersed in a second solution of $AgNO_3$ stabilized with CTAB. In this growth solution, AgNPs deposited on the ITO surface will auto-catalytically react with the second generation of CATB-stabilized Ag nanoparticles thus leading to additional growth of the silver nanoparticles on ITO surface.

3.1. Effect of the growth time on the formed AgNPs on ITO surface

Fig. 1 shows the FE-SEM images of the AgNPs grown on the ITO-A substrate at various growth times, prepared from Ag nanoseed solution using in situ method based on seed-mediated growth strategy (see Section 2). The time of immersion was found to be very crucial for controlling the size and space uniformity of the nanoparticles as illustrated in the case of ITO-A (Figs. 1 and 2).

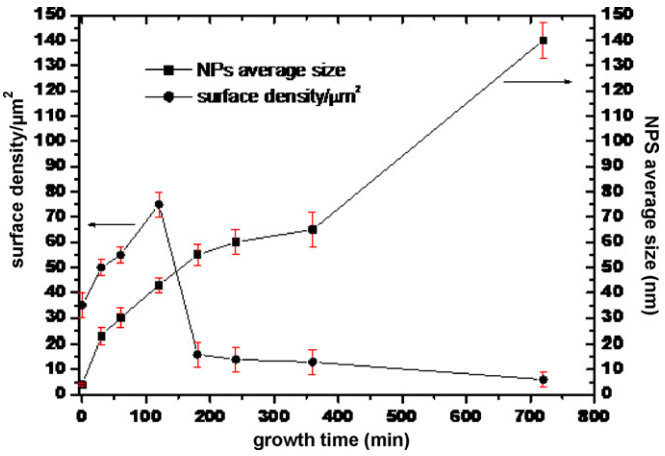

Fig. 2. Average AgNPs size and surface density as a function of growth time (ITO-A).

Just after seeding without growth treatment, the attached Ag nano-seed particles were very small, with dimensions smaller than 4 nm. The obtained AgNPs from the seed step cannot be observed by FE-SEM directly due to resolution limitations of the FE-SEM apparatus (Fig. 1A). Interestingly, by combining seed and growth process, both the evolution of the surface-density attachment and the size of AgNPs on ITO substrate were clearly observed (Figs. 1B–H and 2).

The average size of AgNPs increases with increasing the growth time from 40 ± 3 nm to 140 ± 3 nm (Fig. 2). Extending the immersion time beyond 2 h, the average inter-particular distance decreases significantly with respect to the particle sizes, which leads to important particle–particle surface electrostatic interactions and thus to the coalescence and aggregation phenomena. The net overall result is an increase in particle size and a decrease in the total surface density (Fig. 1E–G). Clearly, the obtained results show that 2 h growth time represents a good balance for a judicious control of particle size and their dispersion-distribution. Therefore, the growth time was fixed at 2 h for the subsequent experiments in order to compare the effect of ITO substrate on the so-formed AgNPs.

3.2. Effect of ITO thickness

To examine the effect of the substrate properties, ITO substrate with three different characteristics referred to ITO-A, ITO-B, and ITO-C were used. Their properties are given in Table 1. The surface roughness, along with the particle size and the quality of size dispersion-distribution were systematically examined by SEM and AFM analyses.

Fig. 3 shows SEM images of the surface morphologies of AgNPs grown on different ITO films with a growth time fixed at 2 h. For comparison purposes, typical representative particle sizes are also included in the figure. SEM images show that ITO-A is characterized by a more uniform surface with a slightly lower roughness than ITO-B and ITO-C. This results in Ag particles that are larger in size but more uniform than the particles that were grown on ITO-B and ITO-C.

The observed differences are attributed to the cavities existing between large grains and subgrains of ITO. In these conditions, initially, two, three or four silver nano-nuclei could be readily produced in a narrow region depending on the free space volume existing between such grains. As the nano-nuclei grow further in the existing confined space, they start to bond and their growth becomes physically restrained as the particles start to impinge on other neighboring particles. As a result, each aggregate is generally larger in size than the individual microspheres, as observed in Fig. 3 (ITO-C).

Fig. 4a–c show the AFM images ($3\ \mu m \times 3\ \mu m$) of ITO-A, ITO-B and ITO-C, respectively. The three sputtered ITO films display different characteristic surface morphologies of grain and sub-grain structures. The ITO root-mean-square (RMS) roughness gives pertinent information about the fine-scale fluctuations in the effective surface height. It is given by the cross-sectional contour plots from AFM images (not shown). The RMS is directly related to both the grain boundary density and the grain size and can generally be determined by two factors: (i) number of grain's boundaries, and (ii) size of the grains. So, as the films thickness increases, the grain boundaries decrease and ITO's grain size increases, which explain the decreased electrical resistivity and contact angle with films thickness (see Table 1). The additionally performed control of their homogeneity has shown that the space non-homogeneity does not exceed 3%.

AFM 3D-images of Fig. 4 show that ITO surface topography is changed with the ITO type, with large disparities in the surface roughness and the features of the grains in terms of their fineness, their orientation and consequently of the total available surface area. Additionally, it was observed (see Table 1) that an increase in ITO films thickness is accompanied with a decrease in the electrical resistivity that drops from 8.58×10^{-4} to 0.77×10^{-4} and then to $0.61 \times 10^{-4}\ \Omega$ cm. This is due to the decrease in surface area of the ITO boundary grain and sub-grain numbers as well as an increase in their average size. Consequently, as the ITO film thickness increases, the size of ITO grains increases, which in turn decreases ITO the total surface area of the grain boundaries and so the contact angle decreases (see Fig. 5). This phenomenon clearly affects the ITO structure in terms of the lattice distortion [23,24], which remarkably decreases with the thickness.

Fig. 6a–c displays GXRD spectra of ITO substrates and their corresponding high resolution surface morphology SEM. ITO peaks around 30.40° and 35.30° were indexed on the basis of cubic structure (JCPDS N 71-2194) to (2 2 2) and (4 0 0) plans, respectively. The lattice parameter was found to be equal 10.12 Å. It is clearly observed that with increasing films thickness, the peak intensity I_{222} decreases, while the peak intensity I_{400} increases, involving preferred orientation along the (4 0 0) plane for ITO-C, which implies that the film was more crystallized. The peak intensity ratio I_{222}/I_{400} variation of GXRD for the three ITO substrates is presented in Table 1. This variation agrees well with the observed surface morphology in Figs. 4 and 6. In fact, ITO-A presents a large grain's boundaries and regular size dispersion of grains and sub-grains ca. 20 nm and 80 nm, respectively. While the grain boundaries in ITO-B and ITO-C decrease, the mean grains and subgrains size dispersion becomes larger (ca. 40 and 400 nm for ITO-B, and ca. 60 nm and 600 nm for ITO-C). Our results are in good agreement with those observed by Qiao et al. [26] and Lee and Park [25]. In fact, Qiao et al. [26] reported that an increase in ITO films thickness generates a decrease in the lattice distortion due to the increase of grains size and the decrease of subgrains. While Qiao et al. associated such a change with the smaller interstitial oxygen incorporated into the crystal lattice, Lee and Park [25] showed that the peak intensity ratio I_{222}/I_{400} decreases gradually with ITO films thickness.

During the seed-growth process, the lattice variation distortion can directly affect the contact angle [14,27] of the deposited AgNPs, which explains the slightly decrease in the AgNPs average size (r_{Ag}) from 40, 35 to 30 nm and AgNPs size regularity (see Table 2) produced on ITO substrate with different thicknesses and roughness.

The atomic ratio Sn/In calculated from a typical energy-dispersive X-ray spectrum of the different ITO/glass (figure not shown). This technique was applied to evaluate the content of chemical elements through the analysis of corresponding FE-SEM images. The peaks of In, Sn, O and Ag are clearly seen, which confirms the impregnation of Ag particles on the ITO matrix. The corresponding integrated concentration of the composite layer is

Table 1
Measured physical properties of three ITO substrates and sheet resistance and average size of AgNPs particles with 2 h growth time at $T = 28\,^{\circ}C$.

Sample	ITO-A	ITO-B	ITO-C
Average ITO films thickness d (nm)	120 ± 12	215 ± 21	330 ± 25
Contact angle	107	81	78
Sn/In (at.%)	2.63	6.25	5.43
ITO films roughness RMS (nm)	5.07 ± 0.20	4.73 ± 0.20	2.49 ± 0.20
Peak intensities ratio I_{222}/I_{400}	3.55	1.9	0.66
Resistivity of ITO films ($10^{-4}\,\Omega\,cm$)	8.58 ± 0.9	0.77 ± 0.09	0.61 ± 0.07
Sheet resistance of AgNPs/ITO films R_{S2} (Ω/sq)	35.5 ± 0.5	2.0 ± 0.1	0.95 ± 0.5
Average Ag particle size (nm)	43 ± 2	31 ± 5	25 ± 8

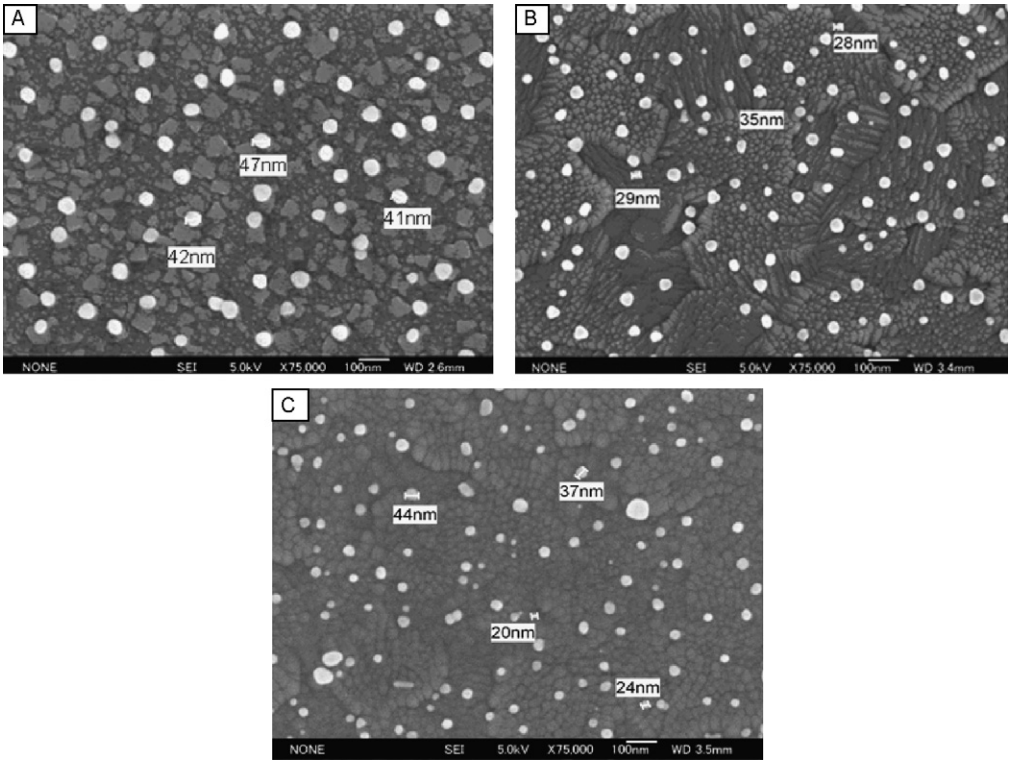

Fig. 3. SEM images of AgNPs grown on: (a) ITO-A, (b) ITO-B, and (c) ITO-C with a sheet resistivity of 71.5, 3.6, and 1.9 Ω/sq, respectively.

also given in Table 1. We can observe from this table, that the ITO roughness is affected by the doping tin content, which influences the growth of AgNPs on the ITO surface as observed in FE-SEM image (Fig. 3). Following this data one can expect that the titled films possess the high stability and is very stable with respect to the oxygen and humidity.

One of the important factors that influence the size of the nanoparticles and their final physical properties is the surface energy and the contact angle during the seed and growth process that is influenced by the initial substrate roughness. In fact, the smoothness of the ITO substrate surface helps solution wetting and spreading, which results in large particle size (Figs. 3 and 5). The contact angle of ITO-C is two times smaller than the ITO-A (Table 1), and FE-SEM (Fig. 3) which explain the irregularity observed in ITO-C. Indeed, during the process, the solution undergoes dewetting and then crystallization, but the numerous generated small domains suffer from small inter-domain distance and interact via van der Waals forces and Ostwald ripening that favour coalescence. In fact, the molecules at the surface of small particles are energetically not favored with respect to the molecules inside the bulk. To overcome this frustrated and unstable thermodynamic state, the surface molecules will detach from the surface and diffuse to join the neighboring particles, which leads to the increase in particle size. Such a process in somewhat hindered by the substrate roughness. As the film roughness increases, the contact angle increases, and the initial seeds find themselves entrapped in narrow and separated regions. During the growth step, the resulting particles undergo van der Waals and Ostwald ripening only the available valleys of the surface. Reaching the neighboring growing particles is restricted by the surface roughness. This one causes a decrease in

Table 2
Calculated specifications parameters (size, FWHM, λ_{max}, etc.) of the supported AgNPs on different ITO features (2 h growth).

Sample	FWHM (nm)	λ_{max} (nm)	Average surface density (particles/μm^2)	AgNPs size homogeneity
Ag/ITO-A	89	410	64	Very well
Ag/ITO-B	102	411	84	Fairly good
Ag/ITO-C	84	416	50	Fair

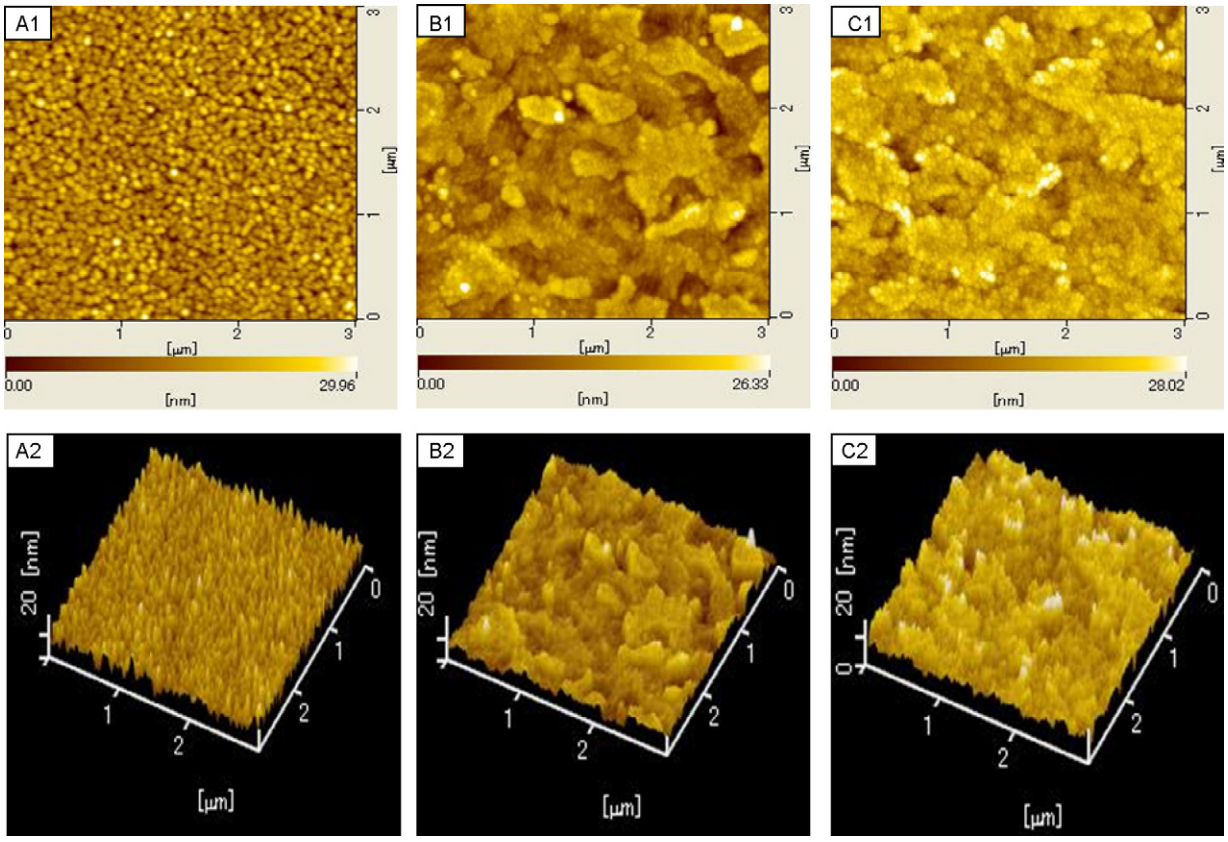

Fig. 4. AFM topography images ((2D) and (3D)) of uncoated ITO-A, ITO-B, and ITO-C substrates.

the particles size with the increase in the substrate surface roughness as shown by the SEM and the AFM micrographs for ITO-A, ITO-B and ITO-C.

This increase in the contact angle can enhance AgNPs sizes for some region of the ITO surface (see the illustrated process in Fig. 7). This scheme illustrates the growth process which occurred on two slightly different rough substrates with homogeneous and inhomogeneous ITO grain size distribution. It shows clearly that the smooth region diminishes the contact angle. As the NPs grow, the aggregation can easily occur due to the Ostwald ripening phenomenon by which the larger AgNPs grow at the expense of the smaller ones [28,29].

This is because the smaller particles grown in large particles are more stable than that deposited on smaller one. Consequently, the substantially smaller particles can detach and diffuse through the solution to form larger particles. This process becomes more favorable with the inhomogeneous ITO grain's nano-size observed in ITO-C. Therefore, the number of smaller particles continues to dissolve and disappear, while larger particles continue to grow. This big particle which appears in Fig. 3B grows even bigger in Fig. 3C. This fact confirms the existence of the aforementioned phenomenon. This also affects the LSPR maximum as observed in Fig. 8 (curve c) (for more details see Section 3.3).

So, the dense and homogeneous AgNPs sizes observed on ITO-A might be due to a high ratio of small homogeneous ITO grain sizes compared to ITO-B and ITO-C, which present very large ITO grain and subgrain size dispersion. This ITO grains size dispersion are particularly effective in the seeding process, for which the physisorption of Ag nano-seed particles was promoted by the ITO grains size, in particular, for the relatively rugged surfaces as previously observed in AuNPs case [6d].

Consequently, we can conclude that ITO-A with homogeneous cavities is favorable for uniform and dense AgNPs growth on the ITO surface without using any undesirable linker molecule. In con-

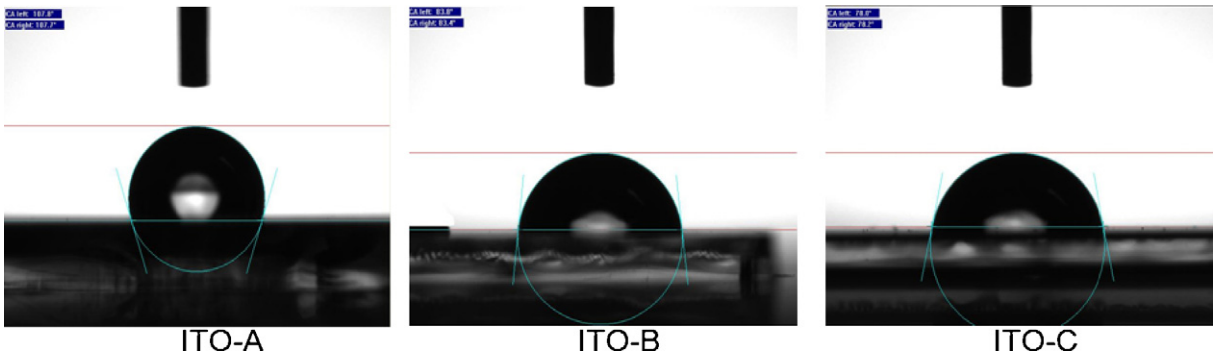

Fig. 5. Contact angle of uncoated ITO-A, ITO-B, and ITO-C substrates.

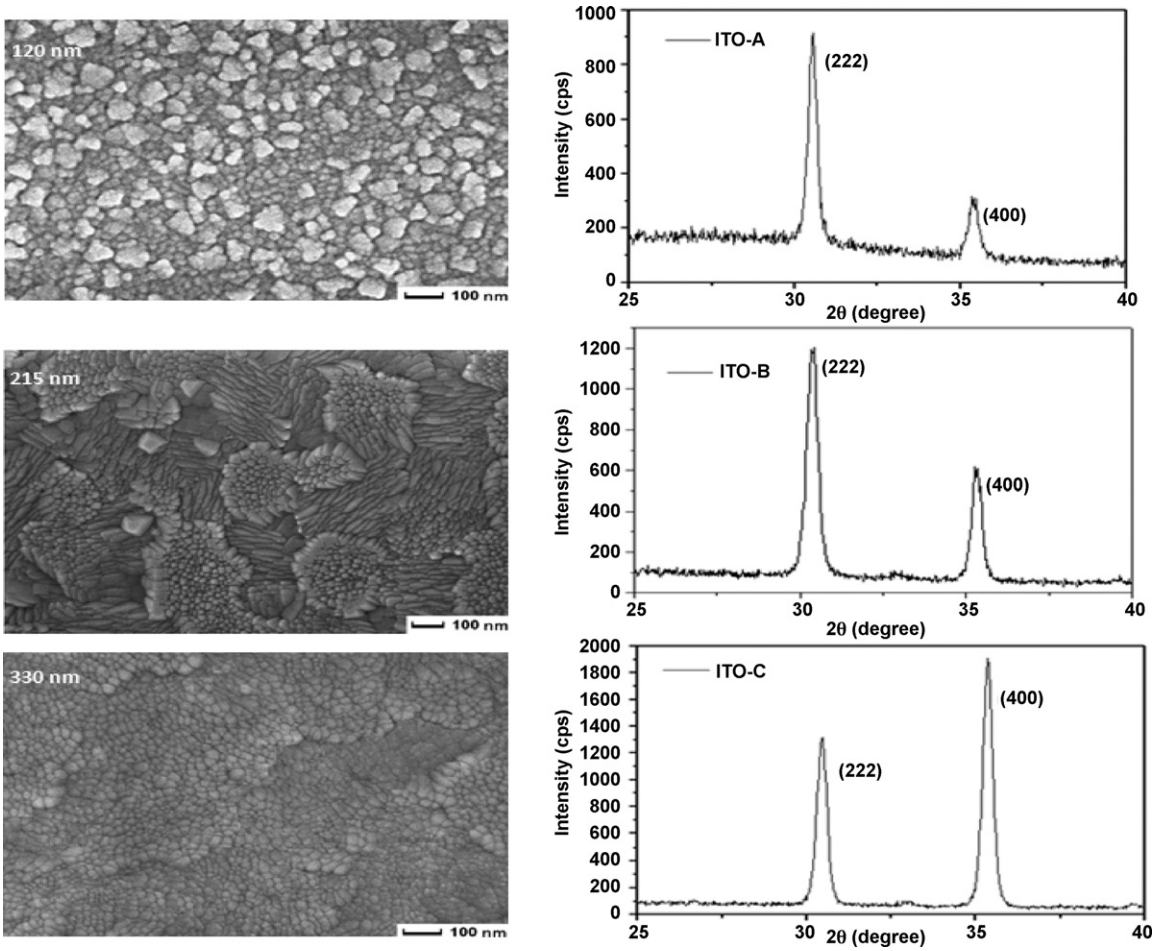

Fig. 6. GXRD spectra of ITO-A (a), ITO-B (b), and ITO-C (c) substrates and their corresponding SEM images.

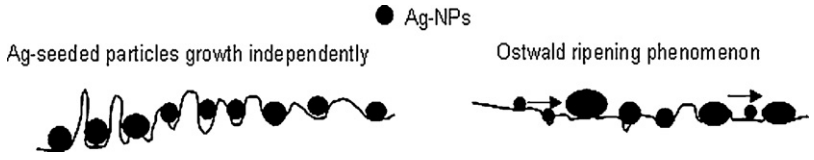

Fig. 7. Schematic representing the AgNPs aggregation by Ostwald ripening phenomenon.

clusion, it is strongly suspected ITO grain and subgrain sizes clearly affect the formation of AgNPs on ITO surface. The homogeneous ITO grain size that is observed on ITO-A with sheet resistivity 71.5 Ω/sq can promote dense and homogeneous nano-size AgNPs of about 40 nm.

3.3. Morphological effect of AgNPs on the absorption spectrum

Fig. 8 presents the UV/visible spectra of AgNP attached on the three ITO surface used in this study. It can be noticed that the maxima of the band absorption are centered at wavelengths of 410, 413 and 416 nm for ITO-A, ITO-B and ITO-C, respectively. They correspond to the LSPR excitation of metal silver NP originating from the collective oscillation mode of the conduction electrons in AgNPs.

The shape of the absorbance curve and resonance peak can be qualitatively related to the morphology of metal nanoparticles on surface [30,31]. In fact, small and uniform size with high surface density presents a sharper absorbance curve, while nanoparticles with wide size dispersion and/or any type of aggregation or coalescence present a broad absorbance curve [33,34]. These λ_{LSPR} lie

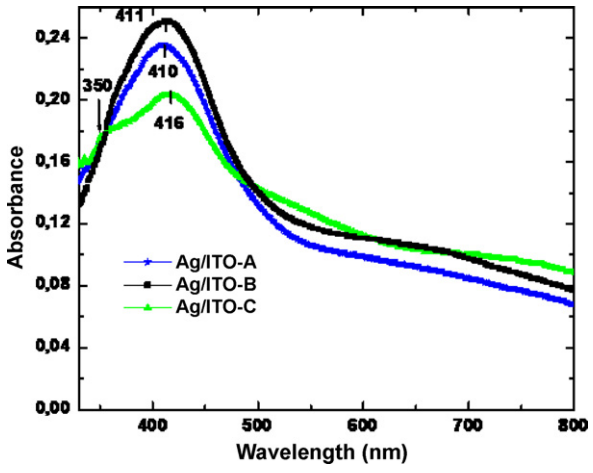

Fig. 8. UV–visible absorbance of AgNPs/ITO-A, AgNPs/ITO-B, and AgNPs/ITO-C for 2 h growth time.

in the same order of wavelengths, recently reported for AgNP prepared by various techniques [35,36]. Besides, the LSPR spectral peak position is shifted to a longer wavelengths with respect to only Ag film (394 nm) [35].

The splitting of the LSPR band (observed in ITO-C) into blue components around 350 nm may be associated with the multi-polar electromagnetic interactions among contacting AgNPs that appear once coalescence starts from smaller AgNPs, and to the quadrupole plasmon resonance and associated to particle geometry [35,37]. The difference in the shape and spectral maximum position of the LSPR band suggests a change in particle size and shape as it is observed in FE-SEM measurements (Fig. 3C).

The average AgNPs size, the full width at half maximum (FWHM), the spectral position of the maximum wavelength λ_{max}, the average surface density and size homogeneity of AgNPs on ITO surface for each sample are shown in Table 2. It is necessary to emphasize that all these parameters for each sample were manually calculated to clearly quantify the various morphologies.

From Table 2 and Fig. 8, one can see that the maximum of LSPR wavelengths λ_{max} is a function of ITO characteristics (composition, thickness). As mentioned in Table 1, the irregularity of the grain sizes depends on the ITO substrate features. The irregular AgNPs size distribution shifts the spectral peak position λ_{max} to the red wavelengths. This can explain the two signals observed for ITO-C. The former at 350 nm is attributed to small silver nanoparticle sizes ($\approx$20 nm) and the second one at 416 nm is caused by the large particles with an average size of 46 nm. Actually, Schatz et al. [38] and Gonzalo et al. [32] reported that the LSPR depends strongly on the particle shape, shifting to the red as the particle becomes more oblate with the appearance of such a smaller peak ca. 398 nm for inhomogeneous shape of AgNPs.

In the above results, some characteristics of AgNPs on ITO such as size, regularity and density prepared by the actual method were highly improved compared with normal seed-mediated growth [6a]. The present AgNPs attachment would be an alternative method to produce regular and dense metals NPs on surface.

The effect of ITO substrate on AgNPs size, regularity and their LSPR response were explicitly presented. The use of rougher/smoother ITO substrates and employing AgNPs with different average particle's sizes are currently under way.

4. Conclusions

This work describes a new chemical approach based on two-steps seed-mediated growth method to fabricate dense and uniform AgNPs on ITO surface. The immersion time in the growth solution was determined as 2 h. The ITO substrate nature with homogeneous cavities is favorable for uniform and dense AgNPs without using any undesirable linker molecule. The attachments of AgNPs on ITO surface as well as their homogeneity are significantly improved on relatively rugged surface which is formed by smaller ITO grains sizes, while smooth ITO surface with larger grains and subgrains size favour smaller and irregular AgNPs size. Additionally, we demonstrated that the UV–visible absorbance spectroscopy curve and LSPR band of AgNPs are very sensitive to their size, density and surrounding particles.

Acknowledgements

We thank Dr. Hiroyuki Nishinaka and Dr. Abdelkrim El Kadib for fruitful discussions and comments. The financial support from Japan Society for the Promotion of Science (JSPS) program is gratefully acknowledged.

References

[1] G. Schmid, Nanoparticle: From Theory to Application, Wiley-VCH Verlag GmbH & Co. KGaA, 2004, ISBN 3-527-30507-6.
[2] C. Rao, A. Muller, A. Cheetham, The Chemistry of Nanomaterials, Synthesis, Properties and Applications, 2003, ISBN 3-527-30686-2.
[3] A. Panacek, L. Kvitek, R. Prucek, M. Kolar, R. Vecerova, N. Pizurova, V. Sharma, T. Nevecna, R. Zboril, J. Phys. Chem. B 110 (2006) 16248.
[4] I. El-Sayed, X. Huang, M. El-Sayed, Nano Lett. 5 (2005) 829.
[5] L.M. Liz Marzan, I. Lado-Tourino, Langmuir 12 (1996) 3585.
[6] (a) G. Chang, J. Zhang, M. Oyama, K. Hirao, J. Phys. Chem. B 109 (2005) 1204; (b) J. Zhang, M. Kambayashi, M. Oyama, Electrochem. Commun. 6 (2004) 683; (c) D. Nkosi, J. Pillay, K. Ozoemena, K. Nouneh, M. Oyama, Phys. Chem. Chem. Phys. 12 (2010) 604; (d) A. Umar, M. Oyama, Cryst Growth Des. 5 (2005) 599.
[7] X. Wang, Y. Chen, Mater. Lett. 62 (2008) 4366.
[8] S. Dubas, V. Pimpan, Talanta 76 (2008) 29.
[9] S. Metraux, C. Mirkin, Adv. Mater. 17 (2005) 412.
[10] H. Lu, S. Liu, X. Wang, X. Qian, J. Yin, Z. Zhu, Mater. Chem. Phys. 81 (2003) 104.
[11] A. Henglein, Langmuir 17 (2001) 2329.
[12] H. Katsuki, S. Komarneni, J. Mater. Res. 18 (2003) 745.
[13] M. Ghoranneviss, F. Yaghobian, M. Farbod, M. Eshghabadi, Curr. Appl. Phys. 9 (2009) S124.
[14] M.S Ulmeanu, M. Zamfirescu, R. Medianu, Colloids Surf. A: Phys. Eng. Aspects 338 (2009) 87.
[15] Z. You, J. Dong, Microelectron. J. 38 (2007) 564.
[16] F. Wong, M. Fung, S. Tong, C. Lee, S. Lee, Thin Solid Films 466 (2004) 225.
[17] K. Aslan, Z. Leonenko, J. Lakowicz, C. Geddes, J. Phys. Chem. B 109 (2005) 3157.
[18] K. Lee, K. Huang, W. Tseng, T. Chiu, Y. Lin, H. Chang, Langmuir 23 (2007) 1435.
[19] I.V. Kityk, J. Ebothe, I. Fuks-Janczarek, A.A. Umar, K. Kobayashi, M. Oyama, B. Sahraoui, Nanotechnology 16 (2005) 1687.
[20] I.V. Kityk, J. Ebothe, K. Ozga, K.J. Plucinski, G. Chang, K. Kobayashi, M. Oyama, Physica E 31 (2005) 38.
[21] J. Sun, Ma. Ding, H. Zhang, X. Lui, X. Han, X. Bao, G. Weinberg, N. Pfander, D. Su, J. Am. Chem. Soc. 128 (2006) 15756.
[22] (a) N.R. Jana, L. Gearheart, C. Murphy, J. Adv. Mater. 13 (2001) 1389; (b) C.J. Murphy, T.K. Sau, A.M. Gole, C.J. Orendorff, J. Gao, L. Gou, S.E. Hunyadi, T. Li, J. Phys. Chem. B 109 (2005) 13857.
[23] M. Kamei, Y. Shigesato, S. Takaki, Thin Solid Films 259 (1995) 38.
[24] L. Hao, X. Diao, H. Xu, B. Gu, T. Wang, Appl. Surf. Sci. 254 (2008) 3504.
[25] H.-C. Lee, O.O. Park, Vacuum 80 (2006) 880.
[26] Z. Qiao, R. Latzb, D. Mergel, Thin Solid Films 466 (2004) 250.
[27] C. Yang, U. Tartaglino, B.N. Persson, J. Phys. Rev. Lett. 97 (2006) 116103.
[28] W.Z. Ostwald, Phys. Chem. 37 (1901) 385.
[29] R. Lorenz, P.W. Voorhees, Growth and Coarsening: Ostwald Ripening in Material Processing, 2002.
[30] G. Xu, M. Tazawa, P. Jin, S. Nakao, Appl. Phys. A 80 (2005) 1535.
[31] C. Song, D. Wang, Y. Lin, Z. Hu, G. Gu, X. Fu, Nanotechnology 15 (2004) 962.
[32] J. Gonzalo, R. Serna, J. Solis, D. Babonneau, C.N. Afonso, J. Phys.: Condens. Matter 15 (2003) S3001.
[33] L.M. Liz-Marzan, Langmuir 22 (2006) 32.
[34] C.L. Schofield, A.H. Haines, R.A. Field, D.A. Russell, Langmuir 22 (2006) 6707.
[35] Y. Song, W. Yanga, M. King, Chem. Phys. Lett. 455 (2008) 218.
[36] T. Ichiro, I. Hideyuki, M. Akihiro, Res. Chem. Intermed. 29 (2003) 939.
[37] V. Ovchinnikov, Microelectron. J. 39 (2008) 664.
[38] K.L. Kelly, E. Coronado, L.L. Zhao, G.C. Schatz, J. Phys. Chem. B 107 (2003) 668.